RSC Advances

ROYAL SOCIETY OF CHEMISTRY

www.rsc.org/advances

Cite this: DOI: 10.1039/c0xx00000x

www.rsc.org/xxxxxx

FULL PAPER

Synthesis, growth, structure and characterization of potassium lithium hydrogen phthalate mixed crystals

J. Vijila Manonmoni, G. Ramasamy, A. Aditya Prasad, SP. Meenakshisundaram and M. Amutha*

* *Department of Chemistry, Annamalai University, Annamalai Nagar – 608002. E-mail aumats2009@gmail.com, Tel. +91 9943114904.*

Received (in XXX, XXX) Xth XXXXXXXXX 20XX, Accepted Xth XXXXXXXXX 20XX

DOI: 10.1039/b000000x

Mixed crystals of lithium-incorporated potassium hydrogen phthalate were grown by the slow evaporation solution growth technique from an aqueous solution containing equimolar quantities of potassium hydrogen phthalate (KHP) and lithium carbonate. Crystal composition, $C_{16}H_{16}KLiO_{11}$ (PLHP), as determined by single-crystal XRD analysis reveals the coexistence of potassium and lithium in the mixed crystal, further supported by energy dispersive X-ray spectroscopy and atomic absorption spectroscopy. It belongs to the monoclinic system with space group $P2_1$ and the cell parameters a = 9.4866 (3) Å, b = 6.769 (2) Å, c = 15.3967 (5) Å, $\alpha = \gamma = 90°$, $\beta = 105.730°$ (3), V = 951.67 (5) $Å^3$ and Z = 2. The relative second harmonic generation (SHG) efficiency measurements reveal that PLHP has an efficiency comparable to that of KHP. The grown crystals were further characterized by single-crystal XRD, FT-IR, SEM/EDS, TGA/DTA, CHN and UV-visible spectral analysis. Hirshfeld surfaces, derived using single crystal X-ray diffraction data, reveal that the close contacts are associated with strong interactions. Fingerprint plots were used to locate and analyze the percentage of hydrogen bonding interactions.

1. Introduction

Potassium hydrogen phthalate (KHP) finds applications in the production of crystal analyzer for long-wave X-ray spectrometer [1,2]. KHP crystals are well known second harmonic generation materials[3] possessing piezoelectric, pyroelectric and electro-optic properties [4-6]. It crystallizes in the orthorhombic system with noncentrosymmetic space group $Pca2_1$[7]. KHP is widely used as Q-switches for Nd:YAG, Nd:YLF, Ti:Sapphire and Alexandrite lasers. The optical, dielectric, thermal properties [8] and structure [9] of lithium hydrogen phthalate have been studied.

Recently, we have investigated the effect of alkali metal sodium doping on the properties of potassium hydrogen phthalate[10], growth, crystalline perfection and characterization of hexaquanickel[II]dipotassium-tetrahydrogen tetra-o-phthalate tetrahydrate[11], hexaquacobalt(II)dipotassium tetrahydrogen tetra-o-phthalate tetrahydrate[12] and nickel(II)-doped hexaaquacobalt(II)dipotassium tetrahydrogen tetra-o-phthalate tetrahydrat [13] crystals. Also, synthesis and crystal structure of $K_{0.78}Na_{1.22}[(C_6H_4COO_4)_2]H_2O$ [14] have been investigated.

Lithium-incorporated potassium hydrogen phthalate $C_{16}H_{12}KLi_3O_{11}$ (LiKP) was synthesized by mixing stoichiometric quantities of phthalic acid, lithium hydroxide and potassium carbonate in the molar ratio of 2:3:0.5. It belongs to the triclinic system with centrosymmetric space group, $P\bar{1}$ [15]. In the present work, we report the synthesis of lithium– incorporated by KHP by

a different route with a varied composition. $C_{16}H_{16}KLiO_{11}$ (PLHP), crystallizes in a noncentrosymmetric space group $P2_1$ and SHG-active. The grown crystals were subjected to various characterization studies which are briefly described below. Here it is established that by synthesising the mixed crystal in a different route with a controlled concentration of additive, one can sustain nonlinearity at the macro level by allowing the specimen to crystallise in a polar space group. The main objective of the investigation is to design a noncentrosymmetric structure by attempting a different route of synthesis, leading to NLO activity. Steering to noncentrosymmetry from centrosymmetry is made possible by changing the growth conditions. As a part of our investigation [10,14,16,17] in the design of KHP based NLO materials, this work was undertaken.

2. Experimental

2.1 Synthesis and crystal growth

The mixed crystal PLHP was synthesized from an aqueous solution containing equimolar quantities of AR grade KHP and Li_2CO_3 in slightly acidic conditions using de-ionized water. After successive recrystallization, the mixed crystals were grown by the slow evaporation solution growth technique. The crystallization took place within 20-25 d and the crystals were harvested. Photographs of as-grown crystals are shown in **Fig. 1**.

2.2 Characterization techniques

The FT-IR spectrum was recorded using a AVATAR 330 FT-IR instrument using the KBr pellet technique in the spectral range 500-4000 cm^{-1}. The powder X-ray diffraction (XRD) analysis was performed using a Philips X'pert pro triple-axis X-ray diffractometer. The data is analyzed by Rietveld method with RIETAN-2000. The surface morphologies of the sample were observed using a JEOL/JSM 5610 LV SEM which has a resolution of 3.0 nm and an acceleration voltage 20 kV with a maximum magnification of 2,00,000. Energy-dispersive spectroscopy (EDS), a chemical microanalysis technique was performed in conjugation with SEM. TGA/DTA were performed using STD Q 600 in the temperature range 0-600^o C in the nitrogen atmosphere (50 mL min^{-1}) at a heating rate of 10^o C min^{-1}. AAS was recorded using VARIAN Model SPECTRAA 220 spectrometer in acetone – air flame. This technique is used to quantify the concentration of the additive present in PLHP using a graphite line as internal standard. CHN analysis was done using Perkin-Elmer 2400 Series CHNS/O Analyser. The UV–DRS spectrum was recorded using a CARY 5E UV–vis spectrophotometer. The SHG test on the crystal was performed by the Kurtz powder SHG method[18]. An Nd:YAG laser with a modulated radiation of 1,064 nm was used as the optical source and directed onto the powdered sample through a filter. The grown crystals were ground to a uniform particle size of 125-150 µm and then packed in a microcapillary of uniform bore and exposed to laser radiation. The output from the sample was monochromated to collect the intensity of the 532 nm component and to eliminate the fundamental. Second harmonic radiation generalized by the randomly oriented micro crystals was focused by a lens and detected by a photomultiplier tube. In order to ascertain the structure, purity and identification of the grown crystal, single-crystal X-ray diffraction data were collected with a specimen of 0.35 x 0.30 x 0.25 mm^3 size cutout from the grown crystals using an Oxford Diffraction Xcalibur-S CCD system equipped with graphite-monochromated Mo Kα (λ=0.71073 Å) radiation at 293 (2) K. The structure was solved and refined by full matrix least squares on F^2 with WinGX software package [19] utilizing SHELXL-2013 modules [20]. The molecular structure was drawn using *ORTEP*-3 and all non-hydrogen atoms were reformed anisotropically. The Hirshfeld surfaces are calculated using the Hartree-Fock (HF) method with 3-21G as basis set.

3. Result and discussion

3.1 *FT-IR*

The FT-IR spectrum of the as-grown specimen is shown in **Fig. S1 (see ESI)**. An absorption band in the region 500-900 cm^{-1} corresponds to the C-H out of plane

deformations of aromatic ring. The C=O stretching frequency appeared at 1670 cm^{-1}. The characteristic vibrational patterns of KHP [21], LiHP [8] and PLHP are given in **Table 1**. A slight shift of some of the characteristic vibrational frequencies could be due to the stress development because of Li incorporation.

3.2 *TGA/DTA*

Thermal studies reveal the purity of the material. The TGA curve shows a single stage weight loss at ~150^{o}C due to loss of water molecule and there is no further weight loss upto ~420^{o}C. In DTA,the broad endothermic peak at 420 ^{o}C, is due to decomposition. The residual mass observed from thermogram at 600 ^{o}C is ~50% (**Fig.S2**).

3.3 *SEM / EDS*

The SEM micrographs give information about the surface morphology and it is used to check the imperfections [16]. The SEM pictures of PLHP at different magnifications are shown in **Fig.2**. It shows highest surface roughness in a plate like structure, due to defect centers and crystal voids. The presence of Li and K in the PLHP crystal lattice is confirmed by energy dispersive spectroscopy (EDS) (**Fig S3**).

3.4 *AAS and CHN*

Atomic absorption spectroscopic studies were carried out to quantify Li (20.6ppm) and K (21.5 ppm) in the sample. Also, CHN elemental analysis was performed to estimate the quantity of carbon and hydrogen present in PLHP. The elemental composition found was: C 42.93 %, H 3.29%. The calculated composition was: C 44.63%, H 3.7%.

3.5 UV-visible

The UV-visible spectrum of the mixed crystal PLHP reveals high transmittance in the visible region and the lower cut-off wave length is observed at ~300 nm. Incorporation of foreign metal ion into the KHP crystal lattice does not destroy the optical transmission of potassium hydrogen phthalate.

The concentration of an absorbing species can be determined using the Kubelka-Munk equation [22] correlating reflectance and concentration,

$$F(R) = (1-R)^2 / 2R = \alpha / s = Ac / s$$

where F(R) is Kubelka-Munk function, R is the reflectance of the crystal, α is absorption coefficient, s is scattering coefficient, A is absorbance and c is concentration of the absorbing species. The direct band-gap energy of the specimen is estimated as 4.05 eV, from the Tauc plot $[F(R)h\upsilon]^2$ *versus* hυ (eV) (**Fig. S4**).

3.6 *X-ray diffraction analysis*

The powder XRD pattern of PLHP shows that the sample is of a single phase without a detectable impurity. Narrow peaks indicate the good crystallinity of the material. At room temperature all the observed reflections were indexed. The indexed powder XRD pattern is shown in **Fig.3**. Peak positions in powder XRD match with simulated XRD patterns from single crystal XRD. The relative intensity variations could be due to the preferred orientation of the sample used for diffractogram measurement. Also, the mosaic spread of powder and single crystal patterns may differ, resulting in intensity variations. The structure of PLHP is elucidated and the *ORTEP* is given as **Fig.4a**. Three-dimensional view of intramolecular hydrogen bonding interactions is displayed in **Fig.4b**. The crystallographic parameters of LiHP, PLHP, KHP and LiKP are listed in **Table 2**. The chemical formula $C_{16}H_{16}KLiO_{11}$ confirms the presence of K and Li in the crystalline matrix, well supported by EDS and AAS. The specimen crystallizes in the monoclinic crystal system with the noncentrosymmetric space group $P2_1$.

The alkali ions are linked to each other by O–H···O hydrogen bonds through the carboxylate oxygen.

The O atoms of the carboxylate group (in phthalate ions) namely O(1)-O(8) are connected to K1, while the lithium ions are connected with central metal ion *via* O(5)-O(6), O atoms of the water molecules. The K-O bond distances range from 2.8311 (19) to 3.207 (8) Å, which is higher than bond distances observed in potassium hydrogen phthalate monohydrate 2.305 (1) –2.597 (1) Å. The Li–O bond distances lie in the range 1.956 (3)–1.968 (3) Å. The aromatic C-C bond distances fall in the range 1.377 (3) – 1.485 (2) Å. The four carboxy C-O distances are almost same and the values are close to that observed for potassium hydrogen phthalate monohydrate [23] and sodium acid phthalate [24]. In LiKP, O(4)–K(1) bond distance lies at 2.7491 Å whereas in our present study, the O(4)–K(1) bond distance is 2.7671 Å. The selected bond angles and bond lengths are given in **Table 3**.

Crystal packing with hydrogen bonding interactions along the b-axis is given in **Fig.5**. Strong intramolecular hydrogen bonding interactions are O(2)-H(2)···O(11) and O(5)-H(5B)···O(3) assembled with distances of 1.77 and 1.86 Å respectively (**Fig 6)**. Weak intermolecular interactions are observed for O(7)-H(7B)···O(10), O(7)-H(7B)···O(11) and O(5)-H(5B)···O(1), with bond distances of 2.41 (2), 2.46 (3) and 3.25 (4) Å respectively (**Table 4**).

3.7 SHG efficiency

In order to confirm the influence of incorporation of lithium on the NLO properties of KHP the pure and mixed crystals were subjected to SHG test with an input radiation of 6.5 mJ/pulse. The outputs give the relative SHG efficiencies of the measured specimens. As seen, the SHG activity of the mixed crystal is comparable with that of KHP (**Fig S5) and it** is quite likely due to the facile charge transfer, not disturbed by Li-incorporation. Although many materials have been identified that have higher molecular nonlinearities, the attainment of second-order effects requires favourable alignment of the molecule within the crystal [25]. It has been reported that the SHG can be greatly enhanced by altering the molecular alignment through inclusion complexation [26] The mixed crystal PLHP grown from an aqueous solution containing equimolar quantities of reactants crystallize in a noncentrosymmetric space group $P2_1$ and SHG-active, whereas when Li is taken in excess in the growth medium the formed mixed crystal LiKP crystallizes in a centrosymmetric space group and hence SHG-inactive [15]. It is interesting to observe that the mixed crystal of KHP synthesized by a different route crystallises in a polar space group. By changing the growth conditions it is possible to attain noncentrosymmetry in preference to centrosymmetry, a required characteristic of an NLO material.

3.8 Hirshfeld surface analysis

The Hirshfeld surfaces of PLHP have been demonstrated in **Fig.7**, by showing *dnorm*, *shape index*, *de* and *di*. The Hirshfeld surface [27-29] surrounding a molecule is defined by points where the contribution to the electron density from the molecule under consideration is equal to the contribution from all the other molecules. For each point on that isosurface, two distances are determined: one is *de* representing the distance from the point to the nearest nucleus external to the surface and second one is *di,* representing the distance to the nearest nucleus internal to the surface. The normalized contact distance (*dnorm*) based on both *de* and *di*. The surfaces are shown as transparent to allow visualization of the molecule around which they were calculated. The circular depressions (deep red) which are visible on the Hirshfeld surface are an indicator of hydrogen bonding contacts and other visible spots in Fig.7a are due to O···Li (3.6%), H···O (14.5%), O···H (15.9%), K···O (2.0%) and Li···O (3.5%) interactions. The short interactions represented by deep red spots in *de* surface (Fig.7c) are O···Li contacts (3.6%). The dominant O···H (14.5%), Li···O (3.5%) and H···H (31.7%) interactions are viewed in *di* surface plots by the bright red area in Fig. 7d. The *shape index* indicates the shape of the

electron density surface around the molecular interactions. The small range of area and light color on the surface represent a weaker and longer contact other than hydrogen bonds. The two-dimensional fingerprint plots [30] of PLHP exemplify the strong evidence for the intermolecular interactions pattern. In the fingerprint region (**Fig.8**), O···H (15.9%) interactions are represented by a spike in the bottom area whereas the H···O (14.5%) interactions are represented by a spike in the top left region. Hydrogen-hydrogen interactions H···H (31.7%) are very high while compared to the other bonding interactions. Sharp curved spike at the bottom left area indicates the O···Li (3.6%) and top left corner with curved spike indicates the Li···O (3.5%). The finger print at the bottom right area represents C···H (11.7%) interactions and top right area represents H···C (8.7%) interactions. The number of interactions in terms of percentage are represented in a pie chart in **Fig.9**.

4. Conclusion

A novel nonlinear mixed phthalate crystal $C_{16}H_{16}KLiO_{11}$ was successfully synthesized and grown from an aqueous solution by the slow evaporation solution growth technique. The structural analysis by single crystal X-ray diffraction analysis confirms the coexistence of K and Li ions in the mixed crystal. The FT-IR studies indicate the lattice stress in the mixed crystal and SEM images reveal the defect centers with crystal voids. Lithium-incorporated KHP exhibits a large SHG efficiency, comparable with that of KHP, optical transparency and reasonable thermal stability. It is established here that it is possible to steer a specimen to crystallize in a polar space group by changing the growth conditions. So that NLO activity can be sustained at the macro level. The intra- and intermolecular interactions, the prime factors responsible for charge transfer leading to nonlinearity, are visualized by a Hirshfeld surface analysis.

References

[1] J. L. Jones, K.W. Paschen and J.B. Nicholson, *J. Appl. Opt.,* 1963, 2, 955-961.

[2] O. Yoda, A. Miyashita, K. Murakami, S. Aoki and N. Yamaguchi, *Proc. Spie Int. Soc. Opt. Eng.,* 1991,1503, 463-466.

[3] N. Kejalakshmi and K. Srinivasan, *J. Phys. D: Appl. Phys.,* 2003, 36, 1778-1782.

[4] A. Miniewicz and S. Bartkiewicz, *Adv. Mater. Opt. Electron.,* 1993, 2, 157-163.

[5] N. Kejalakshmi and K. Srinivasan, *Opt. Mater.,* 2004, 27, 389-394.

[6] M.V.Shankar and K.B.R Varma, *Ferroelectr Lett.,* 1996, 21, 55-59.

[7] Y. Okaya, *Acta Cryst.,* 1965, 19, 879-882.

[8] A. Senthil, P. Ramasamy and G. Bhagavannarayana, *J.Cryst. Growth,* 2009, 311, 2696-2701.

[9] W. Gonschorek and H. Kuppers, *Acta Cryst. Sect., B* 1975, 31, 1068-1072.

[10] G. Ramasamy, S. Parthiban, S.P. Meenakshisundaram and S.C. Mojumdar, *J Therm Anal Calorim*., 2010, 100, 861–865

[11] K. Muthu, G. Bhagavannarayana, S.P. Meenakshisundaram, *Spectochim. Acta Part A.,* 2012, 92, 289-294.

[12] K. Muthu, G. Bhagavannarayana, C.K. Mahadevan, S.P. Meenakshisundaram. *Mater. Chem. Phys.,* 2013, 139, 623-628.

[13] K. Muthu, G. Bhagavannarayana and S.P. Meenakshisundaram, *Solid State Sci.,* 2012, 14, 1355-1360.

[14] G. Ramasamy and Subbiah Meenakshisundaram, *J. Cryst. Growth,* 2013, 375, 26-31.

[15] B. Sivakumar, S. Gokulraj, G. Rameshkumar and R. Mohan, *Bull. Korean Chem. Soc.,* 2012, 33, 3755-3756.

[16] S. Meenakshisundaram · S. Parthiban U. R. Pisipaty · G. Madhurambal · S. C. Mojumdar *J Therm Anal Calorim* (2010) 100:821–826

[17] S. P. Meenakshisundara S. Parthiban G. Madhurambal and S .C. Mojumdar, *Journal of Thermal Analysis and Calorimetry,* Vol. 94 (2008) 1, 21–25

[18] S. K. Kurtz and T.T Perry, *J. Appl. Phys.,* 1968, 39, 3798-3813.

[19] L.J. Farrugia, *J. Appl. Cryst*. 2012, 45, 849-854.

[20] G. M. Sheldrick, (2013). *SHELXL2013*. University of Göttingen, Germany.

[21] R. Ashok kumar, N. Sivakumar, R. Ezhilvizhi and D. Rajan Babu, *Phys, B.,* 2011, 406, 985-991.

[22] P. Kubelka, F. Munk, Ein Beitrag zur Optik der. Farbanstriche, *Z. Tech. Phys*. (Leipzig), 1931, 12, 593–601.

[23] Yu-Feng Li, Tong-Lai Zhang, Jian-Guo Zhang, and Kai-Bei Yu, *Verlag der Zeitschrift fur Naturforschung*. 2003, 58b, 1171 – 1175.

[24] R.A. Smith, *Acta Cryst.* 1975. *B31*, 2345.

[25] S. R. Hall, P. V. Kolinsky, R. Jones, S. Allen, P. Gordon, B. Boshwell, D. Bloor, P.A.Norman, M. Hursthouse, A. Karaulov and J. Baldwin, *J. Cryst. Growth,* 1986, 79, 745-751.

[26] Y. Wang and D. F. Eaton, *Chem. Phys. Lett.,* 1985, 120, 441-441.

[27] M.A. Spackman and D. Jayatilaka, *Cryst. Eng. Comm.*, 2009, 11, 19-32.

[28] F. L. Hirshfeld, *Theor. Chim. Acta,* 1977, 44, 129–138.

[29] CrystalExplorer (Version 3.1), S.K. Wolff, D.J. Grimwood, J.J. McKinnon, M.J. Turner, D. Jayatilaka and M.A. Spackman, University of Western Australia, 2012.

[30] M.A. Spackman and J.J. McKinnon, *Cryst.Eng.Comm.*, 2002, 4, 378-392

Table 1. FT-IR frequencies of some acid phthalate crystals (cm^{-1})

Frequencies	**KHP[a]**	**LiHP[b]**	**PLHP[c]**
υ_{as} (O-H-O)	1090	1072	1089
υ_{s} (O-H-O)	1144	1172	1147
υ_{as} (O-C=O)	1445	1401	1479
γ_{s} (O-C-O)	1565	1552	1531
γ_{s} C=O	1675	1685	1670
γ_{s} O=H	3470	3391	3537

[a]Ref [21] [b]Ref [8] [c] Present study

Table 2. Crystal data of LiHP, KHP, LiKP and PLHP

	LiHP	KHP	LiKP	PLHP
Chemical formula	$LiH(C_8H_4O_4 2H_2O)$	$KHC_8H_4O_4$	$C_{16}H_{12}KLi_3O_{11}$	$C_{16}H_{16}KLiO_{11}$
Unit Cell Parametrs	a=16.837(2)	a=9.61	a=7.405(5) Å	a=9.4866(3) Å
	b=6.822(1)	b=13.32	b=9.878(5)	b=6.7690(2) Å
	c=8.198(2)	c=6.48	c=13.396(5) Å	c=15.3967(5) Å
	α=90°	α=90°	α=71.778(5) °	α=90°
	β=98.85°	β=98.85°	β=87.300(5) °	β=105.730(3) °
	γ =90°	γ =90°	γ=85.405(5) °	γ =90°
Crystal System	Orthorhombic	Orthorhombic	Triclinic	Monoclinic
Space group	Pnma	$Pca2_1$	$P\bar{1}$	$P2_1$
Z	4	4	_	2
Reference	[9]	[21]	[15]	Present Study

Table 3. Selected bond lengths (Å) and angles (°) of PLHP

Atoms	Bondlengths (Å)	Atoms	BondAngles (°)
C(1)–O(1)	1.212 (2)	O(1)–C(1)–O(2)	123.82(16)
C(1)–O(2)	1.313 (2)	O(1)–C(1)–C(2)	122.65(15)
C(1)–C(2)	1.490 (2)	O(2)–C(1)–C(2)	113.52(14)
C(2)–C(3)	1.395 (2)	C(3)–C(2)–C(1)	119.72(16)
C(4)–C(5)	1.377 (3)	C(7)–C(2)–C(1)	120.85(14)
C(7)–C(8)	1.509 (2)	C(5)–C(4)–C(3)	119.77
C(9)–C(10)	1.485 (2)	C(4)–C(5)–C(6)	120.43(17)
C(10)–C(15)	1.399 (2)	C(6)–C(7)–C(2)	118.75(16)
C(8)–O(3)	1.239 (2)	C(6)–C(7)–C(8)	116.49(15)
C(8)–O(4)	1.258 (2)	C(2)–C(7)–C(8)	124.47(4)
C(9)–O(8)	1.222 (2)	O(7)–K(1)–O(6)	85.44 (5)
C(9)–O(9)	1.298 (2)	O(1)–K(1)–O(5)	76.29 (4)
C(16)–O(11)	1.251 (2)	C(7)–C(8)–O(3)	118.89 (16)
C(3)–H(3)	0.93	C(15)–C(10)–O(10)	119.04 (15)
O(1)–K(1)	2.8385 (16)	C(10)–C(9)–O(8)	121.68 (15)
O(8)–K(1)	2.7737(13)	C(2)–C(1)–O(1)	122.65 (15)
O(5)–K(1)	3.207(2)		
O(7)–K(1	2.8331(19)		
O(5)–Li(1)	1.968 (3)		
O(6)–Li(1)	1.956 (3)		

Table 4. Hydrogen bonds geometry for PLHP [Å, °].

	D(D-H)	D(H...A)	D(D...A)	ANGLE (DHA)
O(2)-H(2)...O(11)	0.82	1.77	2.579(2)	167.9°
O(5)-H(5B)...O(3)	0.95(2)	1.87(3)	2.773(3)	159°(4)
O(7)-H(7B)...O(10)	0.88(2)	2.41(2)	3.288(3)	174°(3)
O(7)-H(7B)...O(11)	0.88(2)	2.46(3)	3.122(3)	132°(3)
O(5)-H(5B)...O(1)	0.95(2)	3.25(4)	3.742(3)	115°(3)

Fig 1. Photographs of mixed crystal PLHP

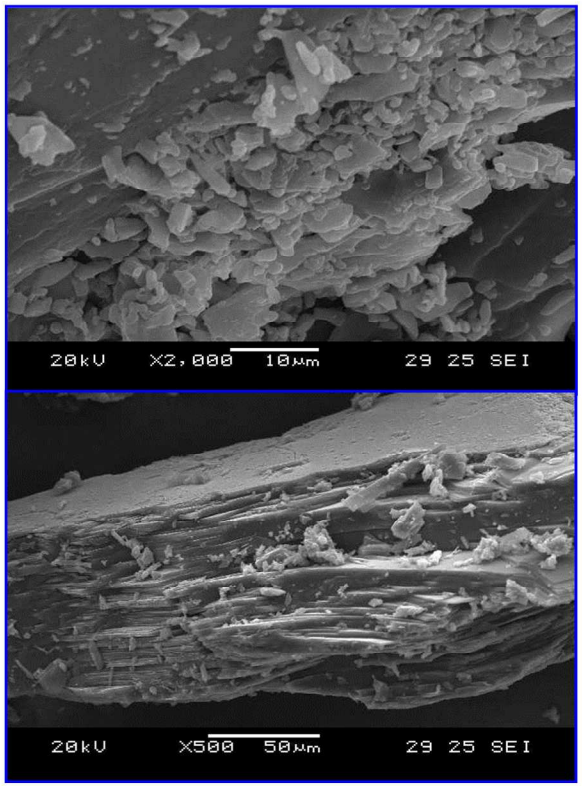

Fig 2. SEM images

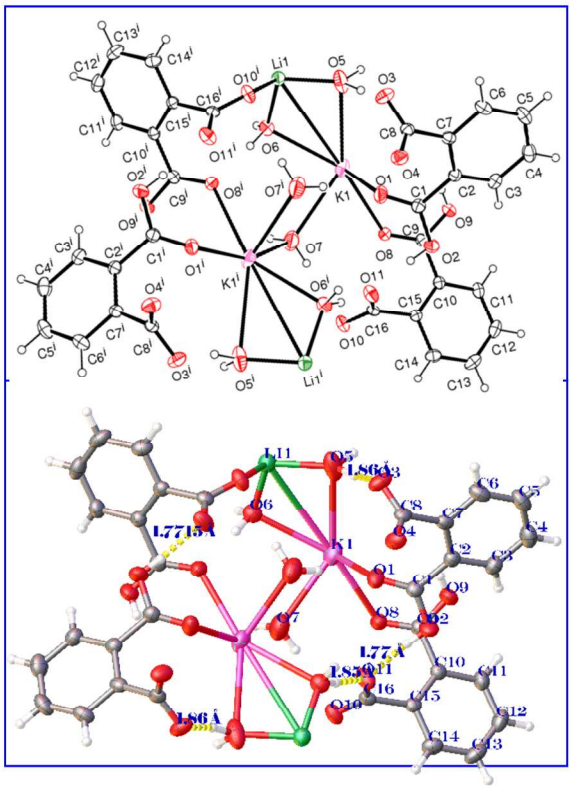

Fig. 4 (a) *ORTEP* of PLHP (b) Three-dimensional view of intramolecular hydrogen bonding interactions (OH···O)

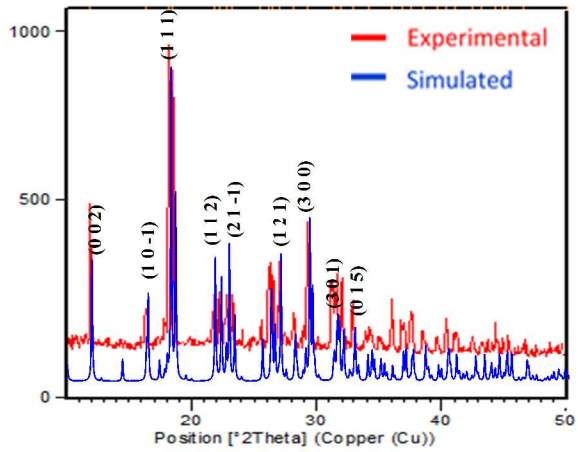

Fig. 3 Experimental and simulated powder X-ray diffraction patterns

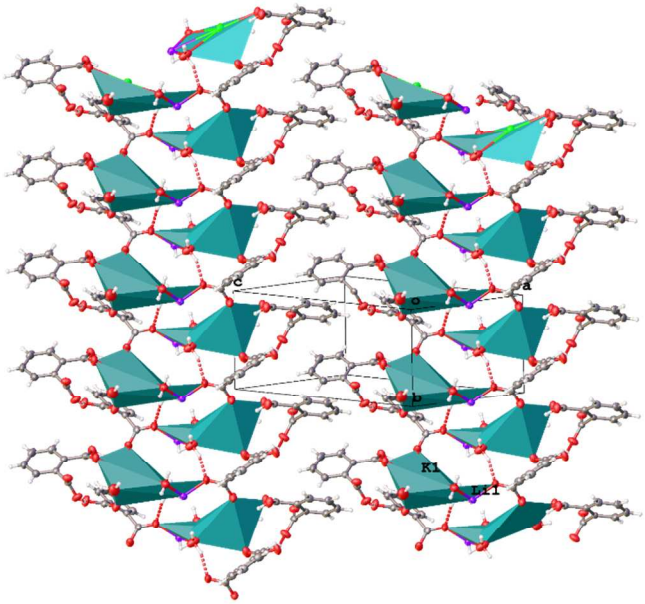

Fig 6. Three-dimensional image of polyhedron with O-H···O interactions

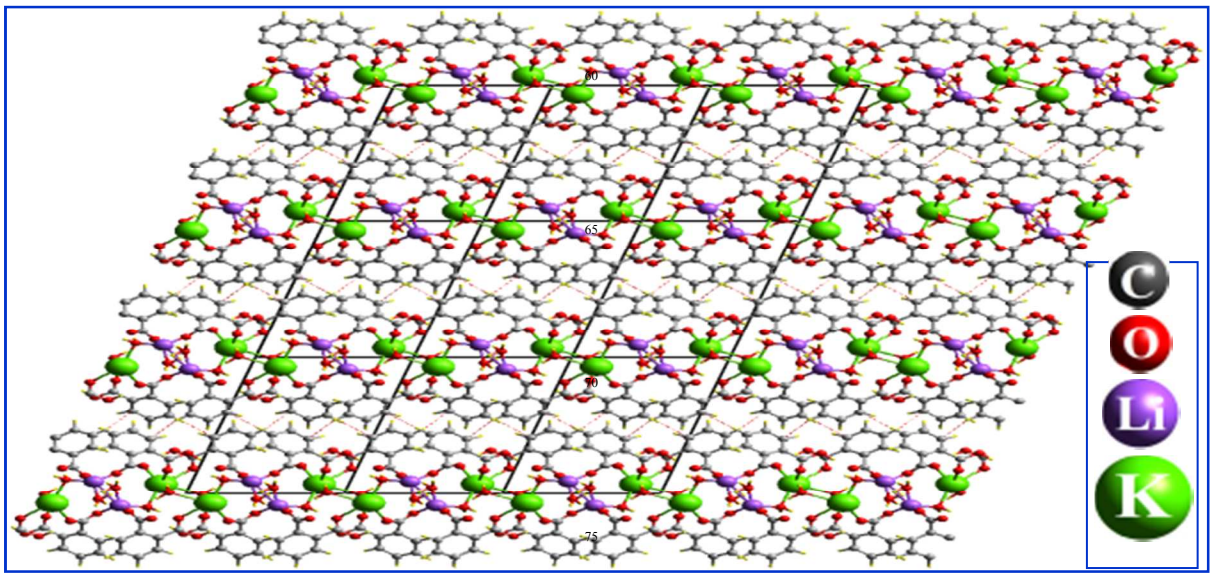

Fig.5 Crystal packing, showing the hydrogen bonding interactions along the b-axis

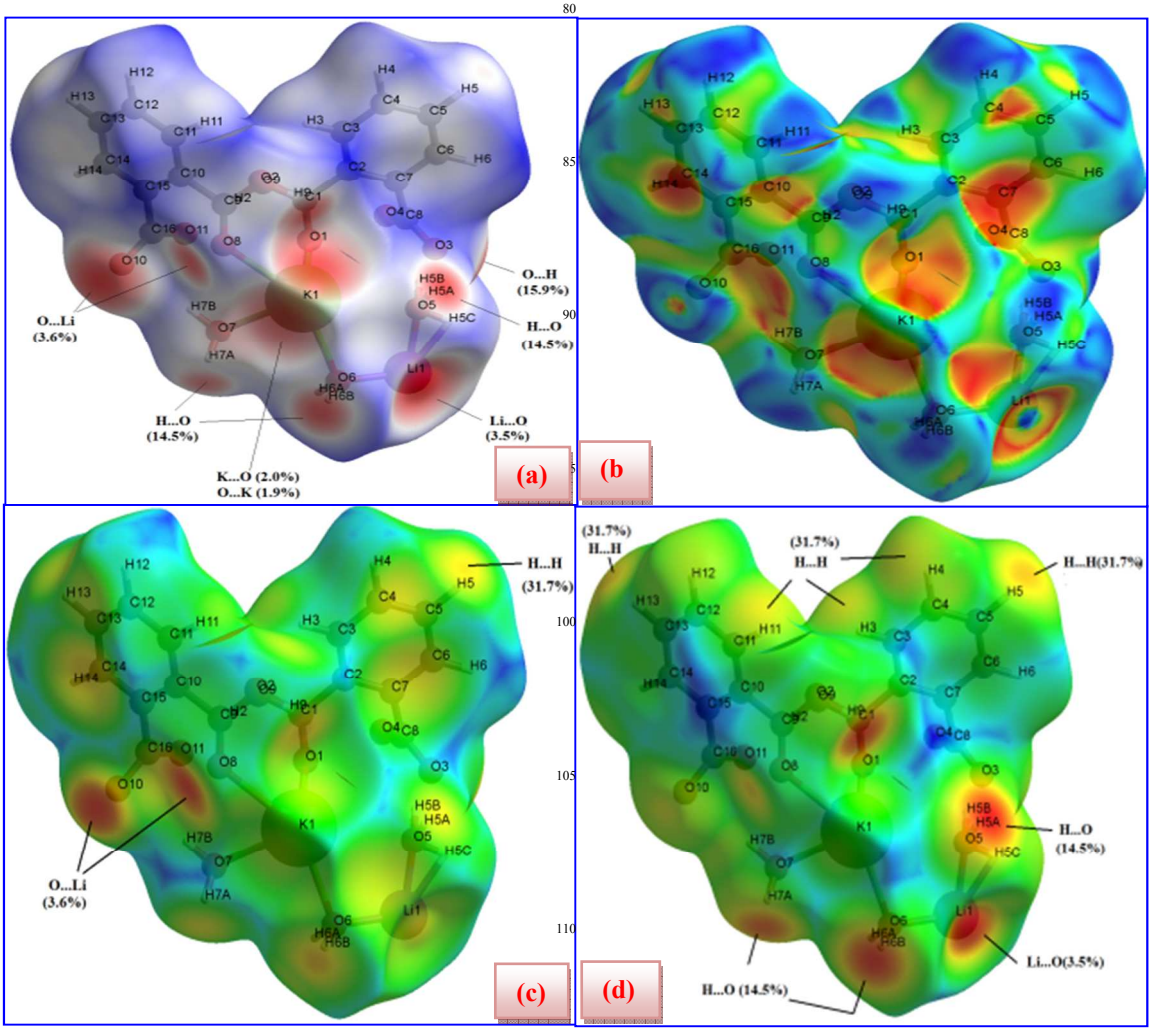

Fig.7 Hirshfeld surfaces (a) *dnorm* (b) *shape index* (c) *de* (d) *di*

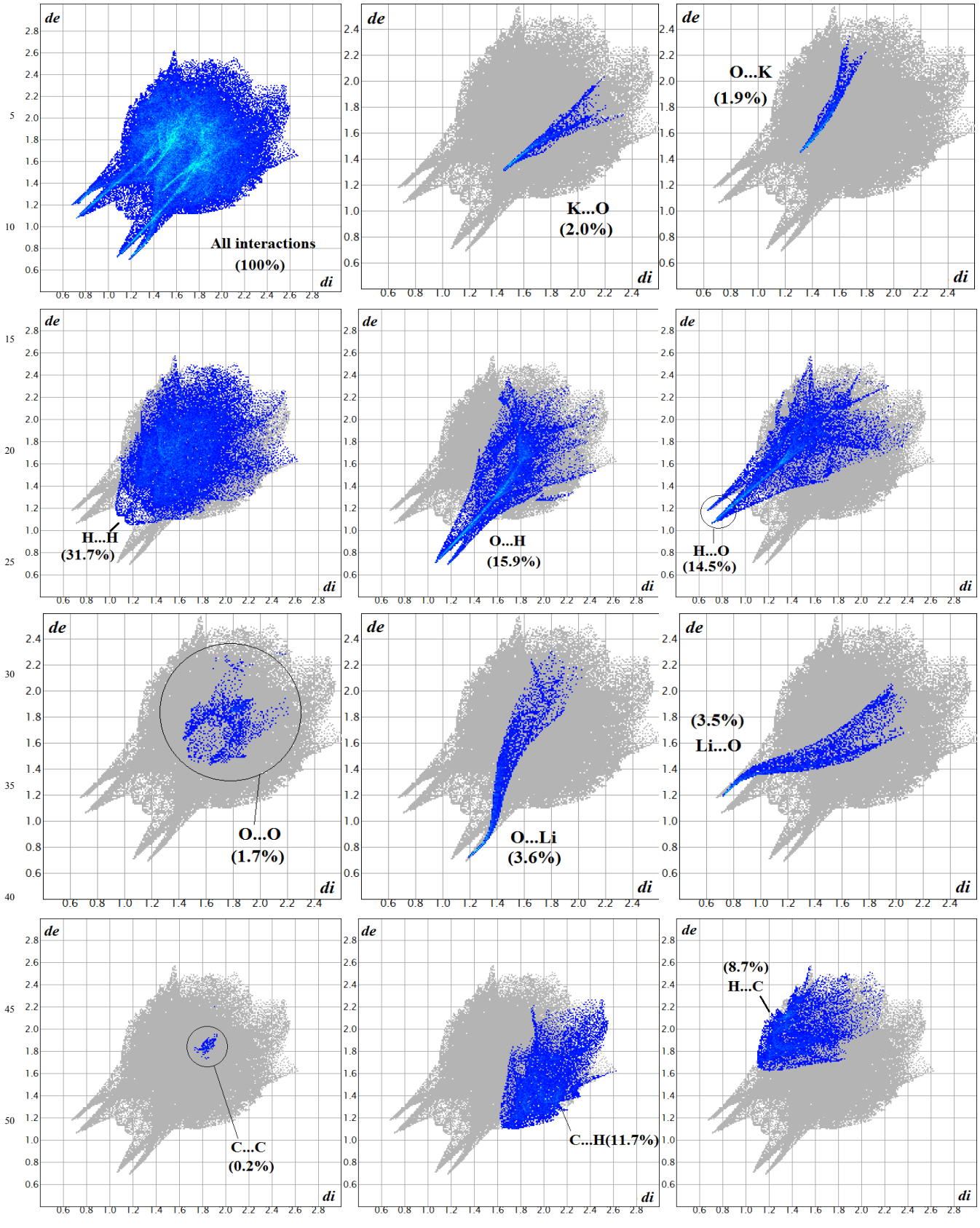

Fig 8. Fingerprint plots

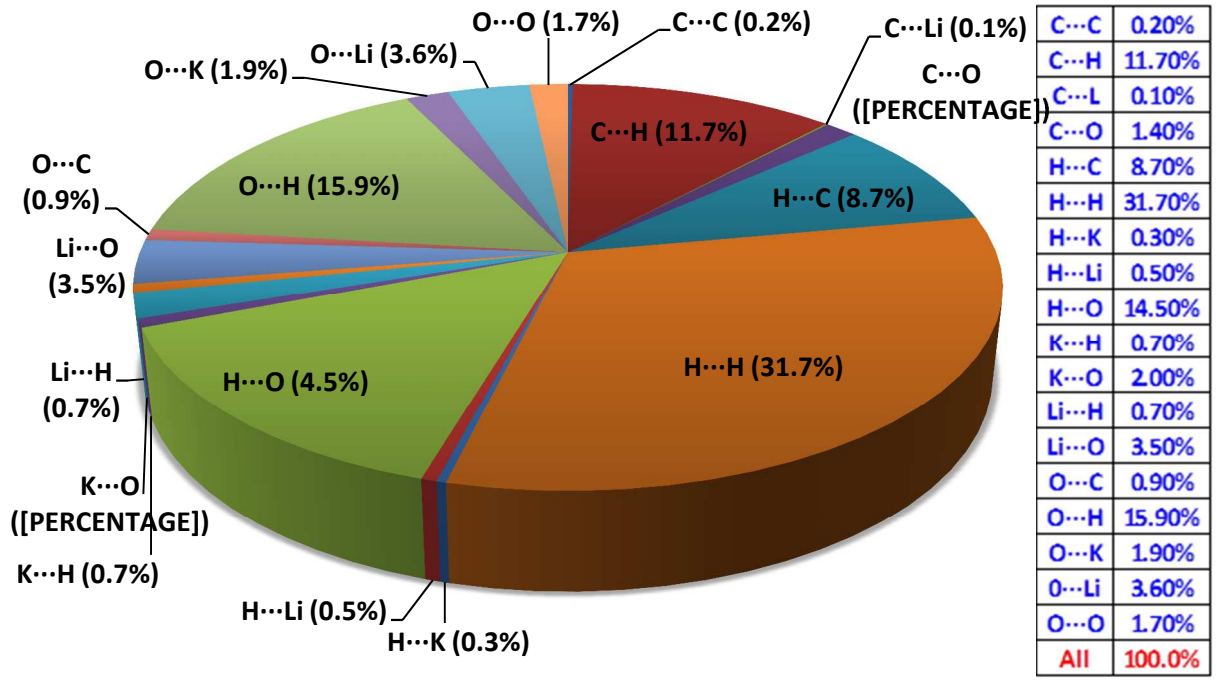

Fig.9 Relative contribution of various intermolecular interactions in PLHP